JOURNAL OF THERMOPHYSICS AND HEAT TRANSFER
Vol. 9, No. 3, July–September 1995

Finite Volume Radiative Heat Transfer Procedure for Irregular Geometries

John C. Chai* and Girija Parthasarathy†
University of Minnesota, Minneapolis, Minnesota 55455
HaeOk S. Lee‡
NASA Lewis Research Center, Cleveland, Ohio 44135
and
Suhas V. Patankar§
University of Minnesota, Minneapolis, Minnesota 55455

A finite volume method for irregular geometries is presented in this article. The capability of the procedure is tested using five test problems. In these tests, transparent, absorbing, emitting, and anisotropically scattering media are examined. The solutions indicate that the finite volume method is a viable solution procedure for radiative heat transfer processes.

Nomenclature

a = coefficient in the discretization equation
b = source term in the discretization equation
D_{ci}^{l} = defined quantities, Eq. (6)
e_b = σT_g^4
I = actual intensity
M = total number of control angles
$\hat{n}$ = outward normal of the control volume faces
$\hat{n}_x$, $\hat{n}_y$ = unit vectors in x and y directions
q = heat flux
q^* = $q/\sigma T_g^4$
s = distance traveled by a beam
S_m^l = modified source function, Eq. (2b)
T = temperature
x, y, z = coordinates directions
β = extinction coefficient, $\kappa + \sigma$
β_m^l = modified extinction coefficient, Eq. (2a)
ΔA = area of the control volume faces
Δv = volume of the control volume
Δx, Δy = control volume widths in x and y directions
$\Delta\Omega$ = control angle, Eq. (6g)
ε = emissivity
η, ξ = curvilinear coordinates
θ = polar angle, Fig. 1
κ = absorption coefficient
σ = scattering coefficient or Stefan–Boltzmann constant
Φ = scattering phase function
ϕ = azimuthal angle, Fig. 1
ω = scattering albedo

Subscripts

b = blackbody
c = cold
E, W, N, S = east, west, north, and south neighbors of P
e, w, n, s = east, west, north, and south control volume faces
g = gas
h = hot
P = control volume P
x, y, z = coordinates directions

Superscripts

l, l' = angular directions

Received March 3, 1994; revision received Oct. 12, 1994; accepted for publication Oct. 31, 1994.

*Ph.D. Candidate, Department of Mechanical Engineering; currently Research Engineer, Innovative Research Inc., 2800 University Ave. SE, Minneapolis, MN 55414. Member AIAA.
†Ph.D. Candidate, Department of Mechanical Engineering. Student Member AIAA.
‡Branch Chief, Icing Technology Branch. Senior Member AIAA.
§Professor, Department of Mechanical Engineering.

Introduction

OVER the last two decades, the control-volume approach[1] has been used in the modeling of fluid flow and heat transfer related processes. Initially, these solutions were performed using Cartesian and cylindrical coordinate systems. A procedure to model irregular geometries using these regular coordinate systems was developed by Patankar[1] and has been used to model irregular geometries successfully. However, this procedure approximates the irregular geometries, and fine grids are sometimes needed to capture complex irregular geometries. To handle irregular geometries with minimal approximation, a number of control-volume fluid flow solution procedures for complex geometries have been proposed. These include the control-volume formulation,[2–6] as well as the control-volume finite element formulation.[7,8]

In the modeling of combined mode heat transfer processes, it is convenient to use a radiative heat transfer calculation procedure capable of sharing the same computational grid with the control-volume computational fluid dynamics (CFD) approach. This eliminates the need to interpolate the temperature and the divergence of heat flux during the iteration process. The procedure presented in this article can also be used even when the radiative transfer grid is different than the fluid flow grid.

Raithby and Chui[9,10] presented a finite volume method (FVM) for radiation heat transfer. A higher-order spatial differencing scheme was used by Raithby and Chui, and their procedure was applied to rectangular and cylindrical enclosures. The procedure was extended to general nonorthogonal coordinates.[11] They employ the computational module used in the control volume finite element method (FEM) of Baliga and Patankar,[7] and Schneider and Raw.[8]

Chai et al.[12] presented a FVM for a Cartesian coordinate system. In this approach, the radiant energy is assumed constant across the entire control surface. The step and modified-

exponential[13] schemes are used as the spatial differencing schemes. Other spatial differencing schemes can also be used. This procedure was tested on two- and three-dimensional geometries. It was shown that the procedure is capable of handling transparent and absorbing-emitting-scattering media. The procedure can also be adapted to model irregular geometries.[14]

Fiveland and Jessee presented finite element[15] and control-volume finite element[16] discrete ordinates methods. Testings of the formulations on irregular geometries are still needed.

The purpose of this article is to extend the procedure presented in Chai et al.[12] to model irregular geometries using general curvilinear coordinates, also known as body-fitted-coordinates (BFC). This procedure is designed to be compatible with the control-volume formulations.[2-6]

The remainder of this article is divided into three sections. The governing equation and the FVM in curvilinear coordinates are presented. This is followed by the presentation and discussion of five test problems. Finally, some concluding remarks are given.

Formulation of the Discretization Equation

The linearized equation of radiative transfer can be written as[12,13]

$$\frac{dI^l}{ds} = -\beta_m^l I^l + S_m^l \tag{1}$$

where the modified extinction coefficient and the modified source term are

$$\beta_m^l = \beta - \frac{\sigma}{4\pi}\Phi^{ll}\Delta\Omega^l \tag{2a}$$

$$S_m^l = \kappa I_b + \frac{\sigma}{4\pi}\sum_{l'=1,l'\neq l}^{L} I^{l'}\Phi^{l'l}\Delta\Omega^{l'} \tag{2b}$$

To discretize the equation of transfer, a finite volume practice is used. The next few sections describe the FVM in curvilinear coordinates.

Design of Control Volumes and Control Angles

In this study, the spatial domain is divided into a finite number of quadrilateral volumes using practice B of Patankar.[1] Figure 1a shows a typical discretized spatial domain. The dashed lines are the boundaries of the control volumes, and the nodal points are located at the center of the control volumes. To avoid clustering, boundary nodes are not shown in Fig. 1a.

The control angles used in this study are the solid angles proposed by Raithby and Chui.[9] These control angles are used by Chai et al.[12] Following the control volume spatial discretization practice, the angular space is subdivided into $N_\theta \times N_\phi = L$ control angles. Figure 1b depicts a sample angular discretization using a unit hemisphere.

Discretization of the Equation of Transfer

Integrating Eq. (1) over a typical two-dimensional control volume Δv (Fig. 2a), control angle $\Delta\Omega^l$ (Fig. 1b), and applying the divergence theorem,[12] Eq. (1) becomes

$$\int_{\Delta\Omega^l}\int_{\Delta A} I^l(\hat{s}^l\cdot\hat{n})\,dA\,d\Omega^l = \int_{\Delta\Omega^l}\int_{\Delta v}(-\beta_m^l I^l + S_m^l)\,dv\,d\Omega^l \tag{3}$$

The left side of Eq. (3) represents the inflow and outflow of radiant energy (within a control angle) across the four control volume faces. The right side denotes the attenuation and augmentation of energy within a control volume and a control angle. Following the practice of the control volume

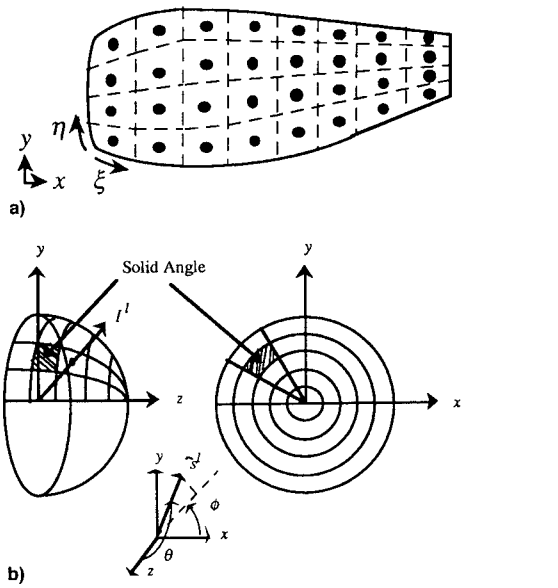

Fig. 1 Samples: a) spatial discretization (boundary nodes not shown) and b) control angle.

approach, the magnitude of the intensity is assumed constant within a control-volume face, a control volume, and a control angle. Under these assumptions, Eq. (3) simplifies to

$$\sum_{i=1}^{4} I_i^l \Delta A_i \int_{\Delta\Omega^l}(\hat{s}^l\cdot\hat{n}_i)\,d\Omega^l = (-\beta_m^l I^l + S_m^l)\Delta v\Delta\Omega^l \tag{4}$$

where $\hat{n}_i$ are the unit outward normal vectors shown in Fig. 2a. In Eq. (4), the radiation direction varies within a control angle, while the magnitude of the intensity is assumed constant. For Cartesian coordinate computation, this practice integrates the zeroth-moment correctly, irrespective of the number of control angles and their arrangement.

In general curvilinear coordinates it is possible to encounter situations with three inflows and one outflow, or vice versa. One such situation is depicted in Fig. 2b. Therefore, the discretization equation should allow for such a situation.

From the experiences of Chai et al.,[17] the step scheme is chosen as the spatial differencing scheme. Other spatial differencing schemes can of course be used. A general discretization equation can be written as

$$a_P^l I_P^l = a_W^l I_W^l + a_E^l I_E^l + a_S^l I_S^l + a_N^l I_N^l + b^l \tag{5}$$

where

$$a_W^l = \max[-\Delta A_w D_{cw}^l, 0], \qquad a_E^l = \max[-\Delta A_e D_{ce}^l, 0] \tag{6a}$$

$$a_S^l = \max[-\Delta A_s D_{cs}^l, 0], \qquad a_N^l = \max[-\Delta A_n D_{cn}^l, 0] \tag{6b}$$

$$a_P^l = \max[\Delta A_w D_{cw}^l, 0] + \max[\Delta A_e D_{ce}^l, 0] + \max[\Delta A_s D_{cs}^l, 0] + \max[\Delta A_n D_{cn}^l, 0] + (\beta_m^l)_P\Delta v\Delta\Omega^l \tag{6c}$$

$$b^l = (S_m^l)_P\Delta v\Delta\Omega^l \tag{6d}$$

$$D_{cw}^l = \int_{\Delta\Omega^l}(\hat{s}^l\cdot\hat{n}_w)\,d\Omega^l, \qquad D_{ce}^l = \int_{\Delta\Omega^l}(\hat{s}^l\cdot\hat{n}_e)\,d\Omega^l \tag{6e}$$

$$D_{cs}^l = \int_{\Delta\Omega^l}(\hat{s}^l\cdot\hat{n}_s)\,d\Omega^l, \qquad D_{cn}^l = \int_{\Delta\Omega^l}(\hat{s}^l\cdot\hat{n}_n)\,d\Omega^l \tag{6f}$$

$$\Delta\Omega^l = \int_{\phi^{l-}}^{\phi^{l+}}\int_{\theta^{l-}}^{\theta^{l+}}\sin\theta\,d\theta\,d\phi \tag{6g}$$

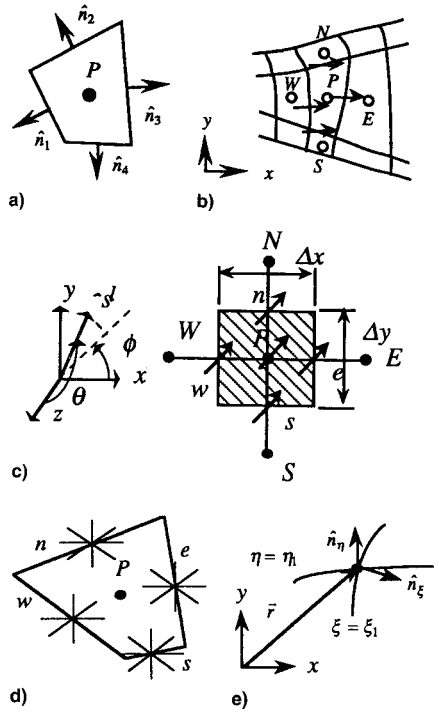

Fig. 2 a) Two-dimensional control volume, b) a possible radiation direction, c) a typical control volume and radiation direction, d) a possible angular discretization in complex irregular geometries, and e) a general point on a curvilinear coordinates line and the position vector *r*.

For the situation shown in Fig. 2c, Eqs. (5) and (6) reduce to

$$I'_P = \frac{\Delta y D'_{cx} I'_W + \Delta x D'_{cy} I'_S + (S'_m)_P \Delta v \Delta\Omega'}{\Delta y D'_{cx} + \Delta x D'_{cy} + (\beta'_m)_P \Delta v \Delta\Omega'} \tag{7}$$

which is the discretization equation reported in Chai et al.[12]

For simple irregular geometries, the control angles can be designed to match the boundaries of a control volume, and Eqs. (5) and (6) are sufficient to describe the problem. However, this treatment is impractical and at times impossible in complex irregular geometries. In such circumstances, the situation depicted in Fig. 2d is almost unavoidable. Since the boundary intensities are approximate in nature, a strict requirement for the interpolation of these control angles does not guarantee added accuracy, but increases the computational time considerably. Therefore, Eqs. (5) and (6) are used as the discretization equation for the nodal intensity.

Treatments of anisotropic scattering and collimated incidence are described by Chai et al.[12] and are not repeated here. Simple irregular geometries can be modeled using the blocked-off region approaches described by Sanchez and Smith[18] and Chai et al.[14]

Other Related Quantities

In this section, the transformation relations from the Cartesian coordinates to a general coordinate system are presented for completeness. Readers interested in a more rigorous presentation on this topic should refer to Thompson et al.[19] or other literature on tensor algebra.

For the purpose of this discussion, Fig. 2e shows a point on a curvilinear coordinate line and the position vector $\boldsymbol{r}$. The unit normal vector $\hat{\boldsymbol{n}}_i$ and the area (with $\Delta\eta = 1$) for the east control surface can be evaluated as

$$\hat{\boldsymbol{n}}_e = \frac{1}{h_\eta}\left(\frac{\partial y}{\partial \eta}\hat{\boldsymbol{n}}_x - \frac{\partial x}{\partial \eta}\hat{\boldsymbol{n}}_y\right), \qquad \Delta A_e = h_\eta \tag{8}$$

where

$$h_\eta = \left[\left(\frac{\partial x}{\partial \eta}\right)^2 + \left(\frac{\partial y}{\partial \eta}\right)^2\right]^{1/2} \tag{9}$$

Similarly, the unit normal vector $\hat{\boldsymbol{n}}_i$ and the area (with $\Delta\xi = 1$) for the south control surface can be evaluated as

$$\hat{\boldsymbol{n}}_s = \frac{1}{h_\xi}\left(-\frac{\partial y}{\partial \xi}\hat{\boldsymbol{n}}_x + \frac{\partial x}{\partial \xi}\hat{\boldsymbol{n}}_y\right), \qquad \Delta A_s = h_\xi \tag{10}$$

where

$$h_\xi = \left[\left(\frac{\partial x}{\partial \xi}\right)^2 + \left(\frac{\partial y}{\partial \xi}\right)^2\right]^{1/2} \tag{11}$$

The volume of a control volume is

$$\Delta v = \frac{\partial x}{\partial \xi}\frac{\partial y}{\partial \eta} - \frac{\partial x}{\partial \eta}\frac{\partial y}{\partial \xi} \tag{12}$$

This completes the formulation of the FVM in general curvilinear coordinates.

Solution Procedure

In the solution of Eqs. (5) and (6), a zero intensity or a suitable intensity field is used as an initial guess. A marching order can be created by examining the position of each control volume relative to its neighbors; however, it is not adopted in this study. In most practical situations, iterations are needed. The practice adopted in this study is to sweep all control volumes from all four corners of the domain. This practice converges rapidly in most situations. A solution is deemed converged when it satisfies the following constraint:

$$|I'_P - I'^0_P|/I'_P \leq 10^{-6} \tag{13}$$

where I'^0_P is the intensity from the previous iteration.

Sample Calculations

All two-dimensional problems reported in Chai et al.[12] were repeated using Cartesian grids. As expected, the solutions reported in the paper were reproduced. In the following sections, five test problems are presented to show the capability of the present procedure. More comparisons can be found in Chai.[20]

Isothermal Absorbing–Emitting Medium in a Square Enclosure

This problem consists of an absorbing–emitting medium maintained at a constant temperature T_g. The black, square enclosure is kept at 0 K, and the absorption coefficient is taken as 10 m^{-1}. The width and height of the enclosure are 1 m.

The spatial domain is discretized into 10 × 10 control volumes in the x and y directions, respectively. The angular domain is discretized into 2 × 8 control angles in the θ and ϕ directions, respectively. Four different spatial grid layouts are used and are shown in Fig. 3. These are an orthogonal and three nonorthogonal grids. Figs. 3b and 3c are designed to study the effect of grid skewness, while Fig. 3d is devised to examine the effect of curvature.

Figure 4 shows the dimensionless heat flux on the left wall obtained using these four spatial grids. It can be seen that the exact solution is reproduced reasonably well using 10 × 10 control volumes. In Fig. 4, the exact solution and the solution obtained using the orthogonal grid show the actual values, and the other curves are displaced for clarity.

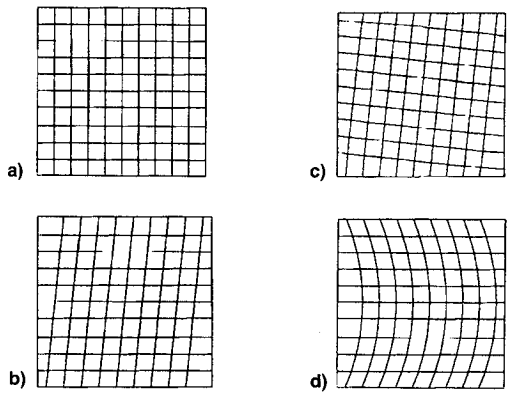

Fig. 3 Four computational grids (all sides are 1 m): a) orthogonal, b) non-1, c) non-2, and d) curved.

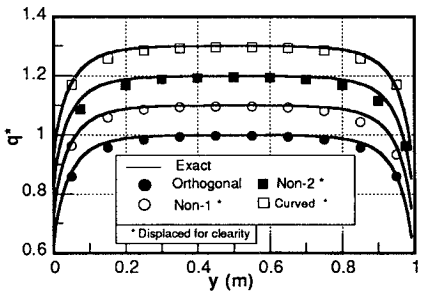

Fig. 4 Dimensionless heat flux on the left wall.

Quadrilateral Enclosure

Figure 5a shows an irregular quadrilateral enclosure (all dimensions are in meters). Similar to the square enclosure, the absorbing–emitting medium is maintained at T_g. The black walls are kept at 0 K and three absorption coefficients, namely, 0.1, 1, and 10 m^{-1} are studied.

Figure 5b shows the dimensionless net heat flux at the bottom wall. These results were obtained using 10 × 10 control volumes and 2 × 8 control angles. It can be seen that the present procedure has captured the physics of the problem with relatively coarse spatial and angular grids.

The CPU times for the above runs were 0.22 and 0.057 s on a 66-MHz Pentium personal computer and Cray C-90, respectively.

Rhombic Enclosure

Figure 6a shows a rhombic enclosure and its computational grid (again, all dimensions are in meters). The bottom wall is hot (e_b = 1), and the other three walls as well as the medium are maintained at 0 K. The medium absorbs and scatters energy. Figure 6b shows the right wall heat flux distributions for two scattering phase functions, (isotropic and F1[21]), and various scattering albedos ($\omega = \sigma/\beta$). In the above studies, the extinction coefficient β is taken as 1 m^{-1}. The spatial and angular domains are discretized into 10 × 10 control volumes and 4 × 16 control angles. Figure 6b shows that the present results compare very well with the Monte Carlo solutions of Parthasarathy et al.[22]

Table 1 shows the CPU times used in the computations. The Monte Carlo method (MCM) CPU times are for a Cray C-90. The FVM CPU times are reported for runs made on 66-MHz Pentium and Cray C-90 computers. Table 2 lists the top wall heat fluxes for two scattering albedos obtained using the MCM and the FVM, respectively.

Curved Geometry No. 1

Figure 7a shows a quarter of a circle with a rectangular region added to the top. The spatial domain is discretized into 35 × 35 control volumes and Fig. 7b shows a sample computational grid. The angular space is discretized into 4 × 24 control angles in the θ and ϕ direction, respectively. The curved wall is hot (e_b = 1), while the other walls are maintained at 0 K. The cold medium (T_g = 0 K) absorbs and scatters energy anisotropically. The F2 phase function of Kim and Lee[21] is used. Figure 7c shows the heat fluxes on the right wall for two scattering albedos ($\omega = \sigma/\beta$). Comparisons with the Monte Carlo[22] solutions are very satisfactory.

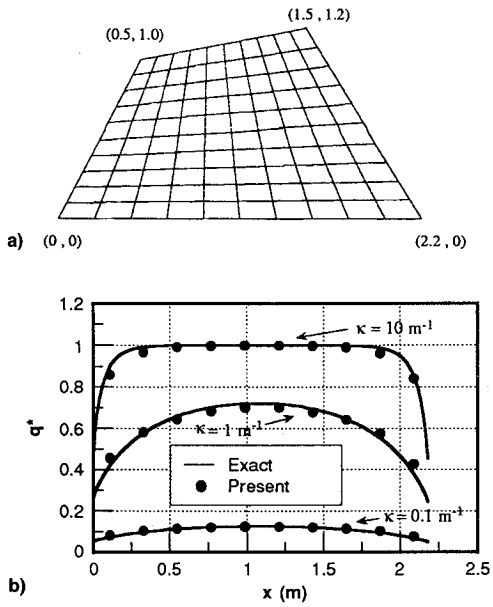

Fig. 5 Quadrilateral enclosure: a) schematic and computational grid and b) dimensionless heat fluxes on the bottom wall.

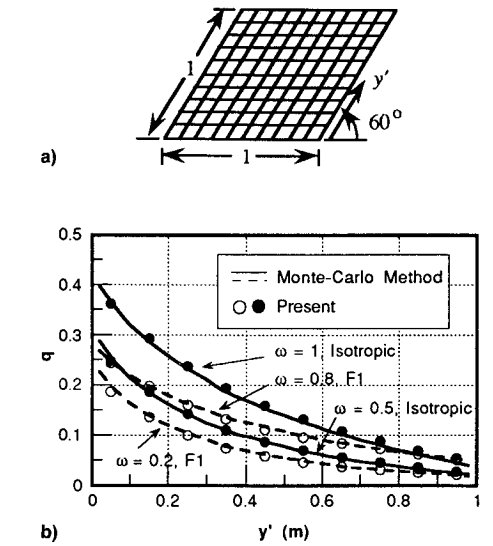

Fig. 6 Rhombic enclosure: a) schematic and computational grid (all lengths are in meters) and b) heat flux distributions at the right wall.

Curved Geometry No. 2

Figure 8a shows the schematic of a test problem commonly used in CFD studies.[3] The top wall is located at y = 1.0 m, whereas the bottom wall varies according to

$$y = \tfrac{1}{2}[\tanh(2 - 3x) - \tanh(2)] \qquad 0 \le x \le \tfrac{10}{3} \qquad (14)$$

Figures 8a and 8b show samples of BFCs and the blocked-off region[14] grids. The bottom black wall is maintained at

Table 1 CPU times[a] for the Monte Carlo and FVMs

ω	Monte Carlo[b]	FVM 10×10[c]	FVM 25×25[c]
0.0	—	0.7/0.2	3.96/1.18
0.5	107.32	7.95/1.07	47.95/5.9
1.0	144.16	11.7/1.59	71/8.82

[a]In seconds. [b]Cray C-90 CPU times. [c]66 MHz Pentium PC/Cray C-90 CPU times.

Table 2 Top wall heat fluxes for a rhombic enclosure

	$\omega = 0.0$		$\omega = 0.5$	
x	MC	FVM	MC	FVM
0.02	0.5221	0.5304	0.3275	0.3298
0.06	0.5583	0.5556	0.3492	0.3468
0.10	0.5739	0.5738	0.3620	0.3592
0.14	0.5878	0.5862	0.3681	0.3678
0.18	0.5928	0.5940	0.3723	0.3735
0.22	0.5957	0.5984	0.3780	0.3768
0.26	0.6026	0.6003	0.3830	0.3874
0.30	0.6077	0.6005	0.3806	0.3785
0.34	0.6049	0.5982	0.3850	0.3775
0.38	0.6020	0.5949	0.3801	0.3753
0.42	0.5932	0.5902	0.3727	0.3720
0.46	0.5869	0.5841	0.3702	0.3677
0.50	0.5728	0.5765	0.3619	0.3624
0.54	0.5657	0.5674	0.3541	0.3559
0.58	0.5600	0.5564	0.3470	0.3482
0.62	0.5416	0.5437	0.3386	0.3392
0.66	0.5212	0.5287	0.3230	0.3287
0.70	0.5041	0.5108	0.3113	0.3164
0.74	0.4775	0.4896	0.2967	0.3019
0.78	0.4617	0.4642	0.2791	0.2849
0.82	0.4287	0.4341	0.2598	0.2651
0.86	0.3944	0.3987	0.2386	0.2421
0.90	0.3504	0.3573	0.2101	0.2159
0.94	0.3086	0.3098	0.1827	0.1864
0.98	0.2358	0.2556	0.1432	0.1534

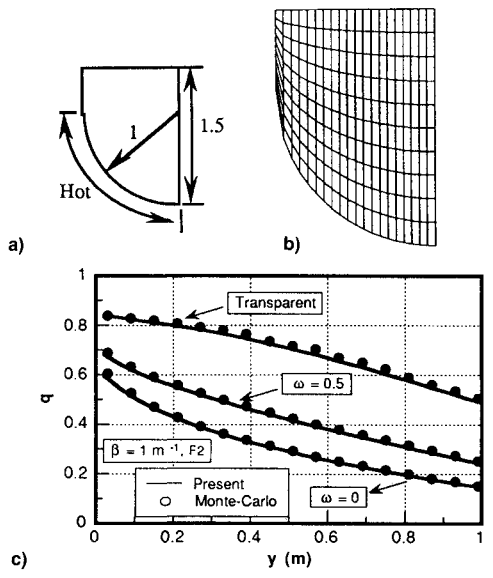

Fig. 7 Curved geometry no. 1: a) schematic, b) BFC grid, and c) heat flux distributions on the right wall.

1000 K while the other black walls are kept at 0 K. The cold (0 K) medium absorbs and scatters energy isotropically with an extinction coefficient of 1 m^{-1}. A total of 40×40 and 40×60 control volumes are used in the present and the blocked-off region solutions, respectively. Both solutions are carried out using 4×24 control angles in the θ and ϕ directions.

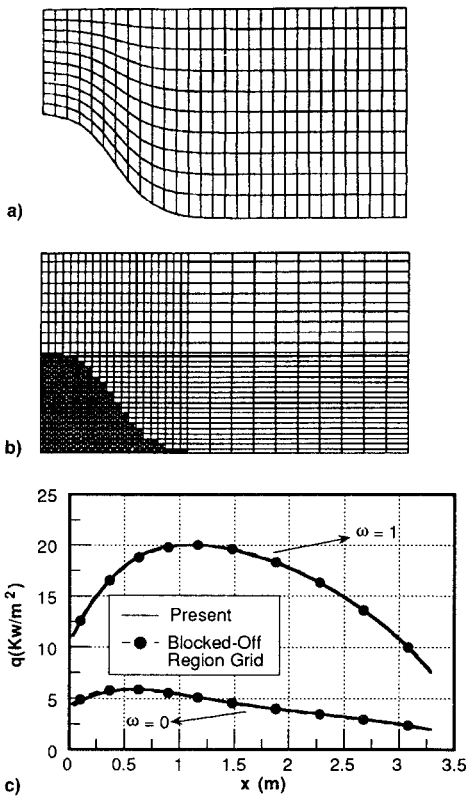

Fig. 8 Curved geometry no. 2: a) BFC grid (all lengths are in meters), b) blocked-off region grid, and c) heat flux distributions on the top wall.

The heat fluxes at the top wall for purely absorbing and purely scattering media show excellent agreements (Fig. 8c).

Concluding Remarks

This article shows that the FVM can be used to model irregular geometries using nonorthogonal control volumes. Using this procedure, control volumes can be designed to capture irregular geometries accurately.

The procedure was applied to five test problems and accurate solutions were obtained. From the basis of the results presented in this article, more extensive testing of the FVM can now be attempted.

Acknowledgments

This work is supported in part by NASA Lewis Research Center under Cooperative Agreement Grant NCC3-238. A Grant from the Minnesota Supercomputer Institute is also gratefully acknowledged.

References

[1]Patankar, S. V., *Numerical Heat Transfer and Fluid Flow*, McGraw–Hill, New York, 1980.

[2]Karki, K. C., and Patankar, S. V., "Calculation Procedure for Viscous Incompressible Flows in Complex Geometries," *Numerical Heat Transfer*, Vol. 14, 1988, pp. 295–307.

[3]Karki, K. C., and Patankar, S. V., "Solution of Some Two-Dimensional Incompressible Flow Problems Using a Curvilinear Coordinate System Based Calculation Procedure," *Numerical Heat Transfer*, Vol. 14, 1988, pp. 309–321.

[4]Kelkar, K. M., and Choudhury, D., "Numerical Method for the Computation of Flow and Scalar Transport Using Nonorthogonal Boundary-Fitted Coordinates," *Numerical Heat Transfer*, Vol. 24, No. 4, Pt. B, 1993, pp. 391–414.

[5]Peric, M., "A Finite Volume Method for the Prediction of Three Dimensional Fluid Flow in Complex Duct," Ph.D. Dissertation, Univ. of London, London, 1985.

[6]Shyy, W., Tong, S. S., and Correa, S. M., "Numerical Recirculating Flow Calculations Using a Body-Fitted Coordinate System," *Numerical Heat Transfer*, Vol. 8, 1985, pp. 99–113.

[7]Baliga, B. R., and Patankar, S. V., "A Control Volume Finite Element Method for Two-Dimensional Fluid Flow and Heat Transfer," *Numerical Heat Transfer*, Vol. 6, 1983, pp. 245–261.

[8]Schneider, G. E., and Raw, M. J., "Control Volume Finite-Element Method for Heat Transfer and Fluid Flow Using Colocated Variables, 1. Computational Procedure," *Numerical Heat Transfer*, Vol. 11, 1987, pp. 363–390.

[9]Raithby, G. D., and Chui, E. H., "A Finite-Volume Method for Predicting a Radiant Heat Transfer in Enclosures with Participating Media," *Journal of Heat Transfer*, Vol. 112, No. 2, 1990, pp. 415–423.

[10]Chui, E. H., Raithby, G. D., and Hughes, P. M. J., "Prediction of Radiative Transfer in Cylindrical Enclosures with the Finite Volume Method," *Journal of Thermophysics and Heat Transfer*, Vol. 6, No. 4, 1992, pp. 605–611.

[11]Chui, E. H., and Raithby, G. D., "Computation of Radiant Heat Transfer on a Nonorthogonal Mesh Using the Finite-Volume Method," *Numerical Heat Transfer*, Vol. 23, Pt. B, 1993, pp. 269–288.

[12]Chai, J. C., Lee, H. S., and Patankar, S. V., "Finite Volume Method for Radiative Heat Transfer," *Journal of Thermophysics and Heat Transfer*, Vol. 8, No. 3, 1994, pp. 419–425.

[13]Chai, J. C., Lee, H. S., and Patankar, S. V., "Improved Treatment of Scattering Using the Discrete Ordinates Method," *Journal of Heat Transfer*, Vol. 116, No. 1, 1994, pp. 260–263.

[14]Chai, J. C., Lee, H. S., and Patankar, S. V., "Treatment of Irregular Geometries Using a Cartesian Coordinates Finite-Volume Radiation Heat Transfer Procedure," *Numerical Heat Transfer*, Vol. 26, Pt. B, 1994, pp. 225–235.

[15]Fiveland, W. A., and Jessee, J. P., "Finite Element Formulation of the Discrete-Ordinates Method for Multidimensional Geometries," *Journal of Thermophysics and Heat Transfer*, Vol. 8, No. 3, 1994, pp. 426–433.

[16]Fiveland, W. A., and Jessee, J. P., "Comparisons of Discrete Ordinates Formulations for Radiative Heat Transfer in Multidimensional Geometries," *Radiative Heat Transfer: Current Research*, HTD-Vol. 276, 1994, pp. 49–57.

[17]Chai, J. C., Lee, H. S., and Patankar, S. V., "Evaluation of Spatial Differencing Practices for the Discrete-Ordinates Method," *Journal of Thermophysics and Heat Transfer,* Vol. 8, No. 1, 1994, pp. 140–144.

[18]Sanchez, A., and Smith, T. F., "Surface Radiation Exchange for Two-Dimensional Rectangular Enclosures Using the Discrete-Ordinates Method," *Journal of Heat Transfer*, Vol. 114, No. 2, 1992, pp. 465–472.

[19]Thompson, J. F., Warsi, Z. U. A., and Mastin, C. W., *Numerical Grid Generation-Foundation and Applications*, North-Holland, New York, 1985.

[20]Chai, J. C., "A Finite-Volume Method for Radiation Heat Transfer," Ph.D. Dissertation, Univ. of Minnesota, Minneapolis, MN, 1994.

[21]Kim, T.-K., and Lee, H. S., "Effect of Anisotropic Scattering on Radiative Heat Transfer in Two-Dimensional Rectangular Enclosures," *International Heat and Mass Transfer*, Vol. 31, No. 8, 1988, pp. 1711–1721.

[22]Parthasarathy, G., Lee, H. S., Chai, J. C., and Patankar, S. V., "Monte Carlo Solutions for Radiative Heat Transfer in Irregular Two-Dimensional Geometries," *Radiative Heat Transfer: Current Research*, HTD-Vol. 276, 1994, pp. 191–199; also *Journal of Heat Transfer* (to be published).